PAPER

Check for updates

Fabrication of 3D objects incorporating peptides covalently attached *via* reversible disulfide linkages with potential for controlled drug release†

Zhongyuan Wan, Wai Hin Lee, Yicheng Wang, Ataulla Shegiwal* and David M. Haddleton ID *

Bioapplication of 3D printing in the fabrication of scaffolding, implants of organ replacements/recovery, *etc.* has been drawing increasing interest due to its capability to replicate complex structures present in organs, *etc*. Alongside the structure and physical properties, the functionality of printed parts is equally important to deliver appropriate materials for this type of application. Herein, complex structures integrated with a reversibly covalently linked peptide have been fabricated with high resolution *via* digital light processing (DLP) type VAT photopolymerization. Bisacryloyl cystamine was synthesized and incorporated into the printer resin to include disulfide functionality in some of the crosslinks. The printed objects were subsequently treated with tris(2-carboxyethyl) phosphine (TCEP) and loaded with covalently bound lanreotide, as an example of a disulfide bearing peptide, *via* a thiol–disulfide exchange. The uptake of lanreotide and subsequent release by a second reductive treatment of TCEP were monitored. This current method was successful in producing objects different structures capable of reversiblly binding functional peptides with the potential for a controlled release profile by adjusting the crosslink density and disulfide content in the objects has been investigated.

Introduction

3D printing has been an upcoming processing method to fabricate objects with the desired geometry and size.[1–3] Among various 3D printing techniques,[1,4,5] digital light processing (DLP) is promising to fabricate 3D objects at low cost and fulfilling technical and instrumental requirements. DLP utilizes a digital micromirror device (DMD) to project light to cure the desired 2D-patterns layer by layer in a reservoir of curable monomer compositions, and obtain a 3D structure controlled by the motion in the *z*-direction.[6–10] Therefore, the printed part is already solidified and self-supporting during the printing process. This is particularly useful for objects involving a complex internal structure,[11–13] where other techniques are inefficient to construct a self-supporting model with a high resolution or fine structure. Moreover, the dimensions and resolutions of DLP are comparable to the internal structures of human organs, which favours its application in the manufacture of tissue scaffolds, artificial organs, and human tissue to implant or replace human parts,[14–18] known as bioprinting.

One of the applications of 3D bioprinting is to fabricate active ingredient-loaded structures or devices to achieve targeted delivery by means of implanting or scaffolding.[19–21] While encapsulation of substance(s) in manufactured objects has been reported,[22,23] it typically suffers from undesired release prior to application and thus a short shelf-life after manufacturing. Moreover, leaching of the active ingredients is also highly dependent on the conditions of the incubation medium, such as temperature, pH, and ionic strength.[24] To mitigate these problems, covalent conjugation, with reversible chemistry as a releasing trigger, will be essential in delivery devices.

Disulfides are naturally present in the form of cysteine–cysteine couplings and can be exploited *via* thiol–disulfide exchange. The conjugated substance remains attached until the subsequent breakage of the −S–S− bond is triggered, preferably by a reducing agent or another thiol at a higher concentration. Reversible thiol–disulfide exchange to capture and release biomolecules through reversible covalent chemical bonds has long been studied,[25–31] and indeed applied in healthcare over the past decades.[32–36] In the patent by 10× Genomics and the later academic literature by Weitz *et al.*,[37,38] a multi-channel microfluidic device was used to produce hydrogel beads with embedded droplets *via* redox polymerization of acrylamide and bisacryloyl cysteamine (BAC) in emulsions. With the incorporation of BAC, the hydrogel bead is

University of Warwick, Chemistry Department, Gibbet Hill, Coventry, UK.
E-mail: d.m.haddleton@warwick.ac.uk

†Electronic supplementary information (ESI) available. See DOI: https://doi.org/10.1039/d3lp00250k

© 2024 The Author(s). Published by the Royal Society of Chemistry

RSC Appl. Polym., 2024, **2**, 415–425 | 415

solubilised *via* chemical reduction by DTT. This allows for the release of the RNA primer in a droplet-in-droplet emulsion to perform DNA barcoding.

Biocompatibles UK Ltd.[39] used BAC, and its carboxylated derivative (BALC), to produce anionic PVA hydrogel beads. Cleavage of the disulfide bond by chemical reduction results in the PVA beads having a higher degree of swelling and allowing for the uptake of cationic drugs and small organic molecules. Subsequently, the beads were transferred to a normal medium to allow the release of loaded drugs. While reversible covalent crosslinking controlled the release rate by the concentration of the reducing agent in the incubation media, in this approach, the encapsulated species is limited to cationic molecules and it is noted that leaching is still observed.

Voit *et al.*[41] demonstrated protein capture and release by a disulfide-functionalized hydrogel array on thin films prepared *via* masked lithography. The BSA protein was successfully captured in the patterned array using a sequential flow of TCEP, deionized water, BSA and PBS buffer in a microfluidic device. The array could be recovered by flowing TCEP solution into the materials to decouple the BSA followed by oxidation by an Fe (III) solution of the –*SH* back to disulfides.[41]

Ravi *et al.*[32] synthesized a hydrogel using acrylamide and BAC, as the sole crosslinker, followed by cleavage of the disulfides with dithiothreitol to obtain a solution of thiol-functionalized polyacrylamide. The polymer solution could be injected, or moulded, to the desired geometry with reversible gelation by the addition of dithiodipropionic acid to re-form the disulfide. Owing to the low toxicity of the reagents, it was said to have potential for use as ocular lens capsules.

Sanyal *et al.* demonstrated cell attachment and protein capture using a hydrogel comprising PEG based methacrylate functionalized with pyridyl disulfide. They also explored the spatial control of these processes using a micropatterned substrate. Later they investigated the fabrication of hydrogels using thiol–disulfide exchange chemistry with functionalized PEG telomers and tetra-arm PEG thiol and exhibited protein encapsulation and high cell viability of the hydrogel.[27,36]

Recently, disulfides have also been incorporated into 3D printing. With the aid of reversible disulfide chemistry, self-healing, covalent adapting networks (CANs), or decomposable materials with complex structures, have been fabricated *via* different 3D printing techniques, including SLA, DLP and extrusion. Huang *et al.* synthesized disulfide-containing poly (urethane diacrylate)s which were used as crosslinkers in DLP 3D printing. The obtained elastomers showed healing properties at 80 °C over 12 h.[17] Amstad *et al.* fabricated a double network hydrogel by photopolymerization of a jammed aqueous suspension of an acrylamido-2-methylpropane sulfonic acid microgel, acrylamide and bisacryloyl cysteamine (BAC) using a syringe extrusion printer. The material showed a flexural strength of 150 MPa, which is comparable to the bulk polymer. It was also shown to be recyclable by reaction with TCEP treatment to recover the microgel suspension.[40] Fellin and Nelson also used extrusion type printing in the fabrication of a hydrogel from a methacrylate end-capped triblock copoly-

mer of poly(isopropyl-*stat*-ethyl glycidyl ether)-*block*-poly(ethylene oxide)-*block*-poly(isopropyl-*stat*-ethyl glycidyl ether) and pyridyl disulfide methacrylate. Owing to the sol–gel transition and the thixotropic behaviour of the pre-polymer this was suitable for nozzle-injected printing and withstanding its shape for post-curing. The obtained hydrogel showed a volume phase-thermal transition and capability for thiol exchange.[31]

Herein, we report the DLP 3D printing of peptide containing objects *via* photopolymerization and its release study. Disulfide functionalized bisacrylamide (BAC) was first synthesized and incorporated into the printing ink composed of hydroxyethyl acrylate to enhance the solubility of BAC. Then the printed parts were treated with TCEP to obtain thiol groups which allows thiol–disulfide exchange with the disulfide containing peptide. The redox-triggered uptake and release of lanreotide, a cyclic disulfide containing peptide, was studied *via* UV-spectroscopy. This work demonstrated a facile and low-cost route to fabricate objects with a complex geometry and peptide-conjugation ability, and its potential to manufacture delivery devices.

Experiment

Materials

Hydroxyethyl acrylate (HEA), poly(ethylene glycol) diacrylate (MW: 700) (PEGDA), lithium phenyl-2,4,6-trimethyl-benzoylphosphinate (LAP), tartrazine, acryloyl chloride and cystamine dihydrochloride were purchased from Sigma-Aldrich. Lanreotide and calcitonin were supplied by Polypeptide Lab. All the materials were used as received. Deionized water was used in all the processes. The synthesis and characterization of bisacryloyl cystamine (BAC) are described in the ESI (Scheme S1 and Fig. ESI 1†).

Resin and ink formulation

Hydrophilic resins were prepared with the formulations shown in Table 1. Hydroxyethyl acrylate (HEA) was chosen here because of its high hydrophilicity to facilitate peptide uptake and release. Furthermore, it enhanced the solubility of BAC in the printing ink. In brief, lithium phenyl-2,4,6-trimethyl-benzoyl phosphinate (LAP) and tartrazine (a yellow dye used to enhance the resolution) were dissolved in deionized water; subsequently the required amounts of poly(ethylene glycol) diacrylate (PEGDA MW: 700) and hydroxyethyl acrylate (2-HEA) were added. The solutions were stirred for 10 min until the liquid phase was homogeneous and subsequently *N,N'*-bisacryloyl cystamine (BAC) was added. Formulations were sonicated for 5 min to ensure dissolution of all of the BAC into the resin solution at ambient temperature and then kept in amber jars, wrapped in aluminium foil, protected from sunlight, and stored at ambient temperature prior to use.

To demonstrate the printability and resolution, formulation *H-3* was chosen to print different structures. For the internal channel model, the object was cleaned by injecting deionized

Table 1 Formulations of the PEG diacrylate/HEA/BAC based resins[a]

Code	HEA/g	PEGDA/g	BAC/mg
A-1	5	1	240
A-2	5	1.2	240
A-3	5	1.5	240
B-1	5	1	160
B-2	5	1.2	160
B-3	5	1.5	160
C-1	5	1	80
C-2	5	1.2	80
C-3	5	1.5	80
C-3	5	2	80
C-4	5	2.5	80
C-5	5	5	80
D-1	5	1	40
D-2	5	1.2	40
D-3	5	1.5	40
E-1	5	5	4
F-1	5	1	2
F-2	5	1.5	2
F-3	5	2	2
F-4	5	5	2
F-5	0	5	2
H-1	5	1	0.2
H-3	5	2	0.2
H-4	5	5	0.2
O-1	5	1	0
O-2	5	1.2	0
O-3	5	1.5	0
PEGDA-Blank	0	5	0

[a] All formulations used the same photoinitiator: lithium phenyl-2,4,6-trimethylbenzoylphosphinate (LAP, 7.57 mg), dye: tartrazine (3.88 mg) and $[H_2O]$ (1.04 g).

water and then cochineal solution for clarity of the internal channel.

3D printing object design and preparation

The size of the printed cylinders was designed for use in standard UV 96 well plate readers, UV-STAR® Microplate, 96 Well, COC, F-Bottom. The calculated total volume = 392 μl with the dimension of the plate reader hole = 7 mm (Fig. 1). Cylinders were printed with 100 nm resolution (layer thickness), with the printing conditions shown in Table 2. Considering the degree of swelling and the different resin fractions, the parameter of the cylinder was modified to be adapted for all formulations (ESI 9†). The objects were printed using a Cellink Lumen X⁺ (DLP type) and reported to give 50 and 100 μm resolutions working at $\lambda = 405$ nm with commercial UV resin formulations from 10 mW cm⁻² to 30 mW cm⁻² light intensity. Due to the increased viscosity of the resin at higher concentrations of PEGDA and BAC, it was necessary to optimize the printing conditions such that complete parts were printed within the entire range of different formulations. The resin in the resin tank
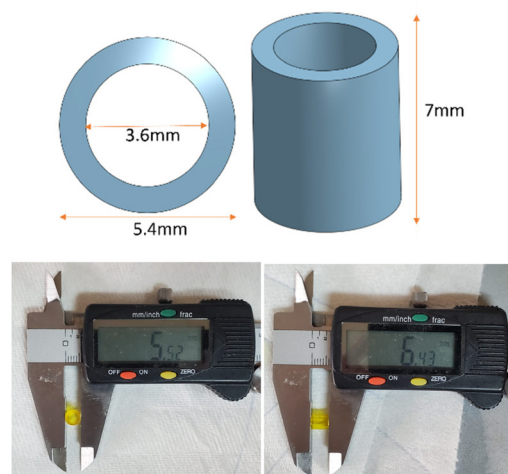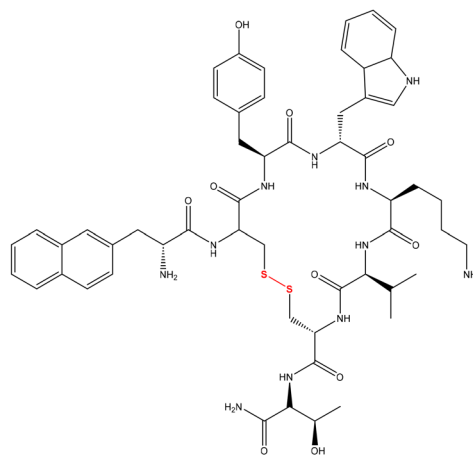

Fig. 1 Design of the 3D printing hydrogels used in the 96 well plate analysis. (H = 7 mm, R = 5.4 mm, r = 3.6 mm), and a sample of the printed model with measured dimensions.

Table 2 Optimization conditions for the Cellink Lumen X + (DLP type) of hydrophilic resin

	Bottom layer	Normal layer
Layer thickness (μm)	100	100
Exposure time (s)	10	10
Light intensity (mW cm⁻²)	25	25

was changed following each print run as the colour of the resin was observed to change and the material properties of the printed parts showed slight differences if this was not carried out.

Procedure for the incorporation of lanreotide into hydrogels

A solution of the peptide lanreotide (Scheme 1) was prepared with 21.93 mg (2×10^{-5} mol) of lanreotide in 40 mL of DI

Scheme 1 Structure of lanreotide used to evaluate the function of the BAC–hydrogel.

© 2024 The Author(s). Published by the Royal Society of Chemistry

RSC Appl. Polym., 2024, **2**, 415–425 | **417**

water and stored in an amber jar at 4 °C. The TCEP-HCl solution was prepared using 143.3 mg of TCEP-HCl in 50 mL of DI water and the solution was stored in amber jars at 4 °C before use.

The printed objects were rinsed three times with 50 ml of DI water to remove any residual resin adhering to the surface of the sample, and then the objects were placed in 50 ml of DI water in an amber bottle for 24 hours to remove the tartrazine and other water-soluble non-crosslinked materials and to ensure that the object was at full hydration. The samples were then dried to remove water from the surface with a clean paper towel. The cleaned and washed cylinders were treated with 1 ml of 10 mM TCEP-HCl diluted with 2 ml of DI water at 30 °C for 2 hours in order to cleave the disulphide bonds within the network and subsequently the object was placed in 70 ml of DI water in an amber bottle for a further 24 hours so as to remove the TCEP from the hydrogel.

Following this, the lanreotide was reacted with the cylinder by adding 160 µL of 0.5 mM lanreotide solution placed in the middle of the hole in the cylinder in a 96 well plate, and the blank reference used was 160 µL of DI water. The UV-Vis absorption at λ = 277 nm, which is λ_{max} for lanreotide, was monitored over 2 hours. Subsequently, the solution remaining in the middle of the hole of the cylinder was removed. 160 µL of fresh deionized H_2O was added into the hole and UV was recorded at λ = 277 nm for a further 30 min. The third stage was to remove the deionized H_2O from within the cylinder and 160 µL of 10 mM TCEP-HCl solution was added with the UV recorded at λ = 277 nm for a further 2 hours.

The hydrogel cylinder was placed in the UV plate during the ensuing reaction processes, and 0.5 mM lanreotide solution was added into the cylinder, while the real working volume was influenced by the volume of the hydrogel and swelling properties which would indicate if the path of light had altered. Corresponding to the Beer–Lambert law equation, if the path of light through the chamber was changed, this would make the absorbance change. In order to obtain an accurate measure of the real path length, the volume was calibrated which could be proportional to the path of light (ESI 4†). The initial amount of 0.5 mM lanreotide solution added was 160 µl, by the calibration to get the real working liquid volume. From the specific volume calculated previously, a new concentration calibration was obtained. The concentration of lanreotide was obtained *via* a calibration using the real working volume calculated previously (ESI 4†).

$$\mathrm{Real\,working\,volume} = \frac{0.5\,\mathrm{mM}}{k_v}$$

$$\mathrm{Real\,concentration} = \frac{A}{k_c}$$

Here, k_v = volume calibration slope (the same concentration, the primary function of absorptivity and volume); k_c = concentration calibration slope (the same volume, the primary function of absorptivity and concentration); and A = real absorbance.

Instrumentation

UV-Vis absorbance. UV-Vis absorbance was measured using a BioTek Synergy HTX Multimode Reader from Agilent. Spectra were recorded from 200 nm to 999 nm with 1 nm increments.

Differential scanning calorimetry (DSC). Differential scanning calorimetry (DSC Mettler-Toledo DSC 1 STAR System) was used to determine the thermal properties of the gels. Standard indium and zinc samples were used to calibrate the temperature and heat flow. Prior to testing, the gels were dried at 40 °C for 48 hours and samples weighing approximately 7 mg were individually weighed. The samples were then equilibrated at −80 °C for 5 minutes and subsequently the temperature was increased at 10 °C min⁻¹ to 150 °C, and then the samples were equilibrated at 150 °C for 5 min. The process was repeated two times, and data were obtained from the second thermal cycle.

Thermogravimetric analysis (TGA). Thermogravimetric data for the dried gels were obtained using a Thermo-analyser Systems device (TA-SDT 650). The specimens weighing approximately 7 mg were weighed individually and heated from 25 °C to 650 °C at a scanning rate of 8 °C min⁻¹.

Reversed-phase high-performance liquid chromatography (RP-HPLC). The released peptide samples were analysed using an Agilent 1260 Infinity II LC System with FLD, PDA and DRi detectors. A reversed phase Kinetex® C18 (5 µm, 2.1 × 50 mm, Phenomenex, Torrance, CA, USA) column was used for HPLC separation with a mobile phase consisting of water (A) and acetonitrile (B), both of which contained 0.1% formic acid. The flow rate was 0.4 mL min⁻¹ and the injection volume was 5 µL. The following elute system was used: 10 → 90% B at 0–2.0 min; 90 → 10% B at 2.0–4.0 min and the completed time is 6 min.

Determination of the degree of swelling. The printed parts were stored in an excess of water for 48 h to reach the fully swollen/hydrated state and then kept in a desiccator at 40 °C for a further 48 h to allow for complete drying/water loss. The mass of the as-printed, fully hydrated and dried objects was measured, and the ratios were used as a normalization measure to evaluate the degree of swelling.

Results and discussion

When the printed cylinders were first swollen/hydrated in water from the as-printed state, there were no obvious trends observed by the eye by varying the amounts of either BAC or PEGDA in the formulations. This was ascribed to the fact that the as-printed objects were partly swollen with unreacted resin already prior to incubation in water. The exchange between water and uncrosslinked soluble monomers made the swelling characteristics at this point complex and analysis difficult. An observation was that the difference between the weights of the cylinders reduced as the [PEGDA] : [BAC] increased, ascribed to the increasing role of PEGDA in the crosslinked network and thus the crosslink densities within the cylinders were similar (Fig. 2). Then from the completely hydrated to the dry states
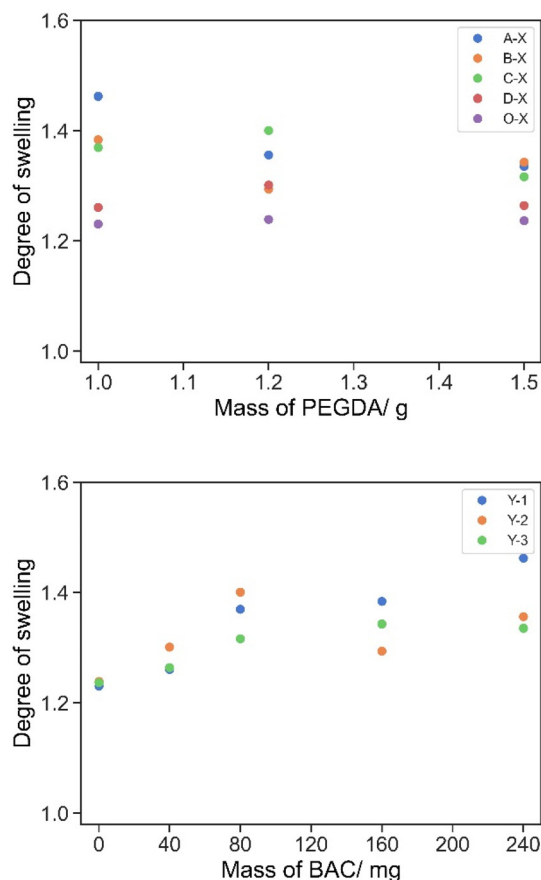
Fig. 2 Degree of swelling for samples A/B/C/D/O-1/2/3 compared with full hydration for 24 hours following printing. Top: grouped by the same BAC content and varying PEGDA contents in the *x*-axis; bottom: grouped by the same PEGDA content and varying BAC contents in the *x*-axis.
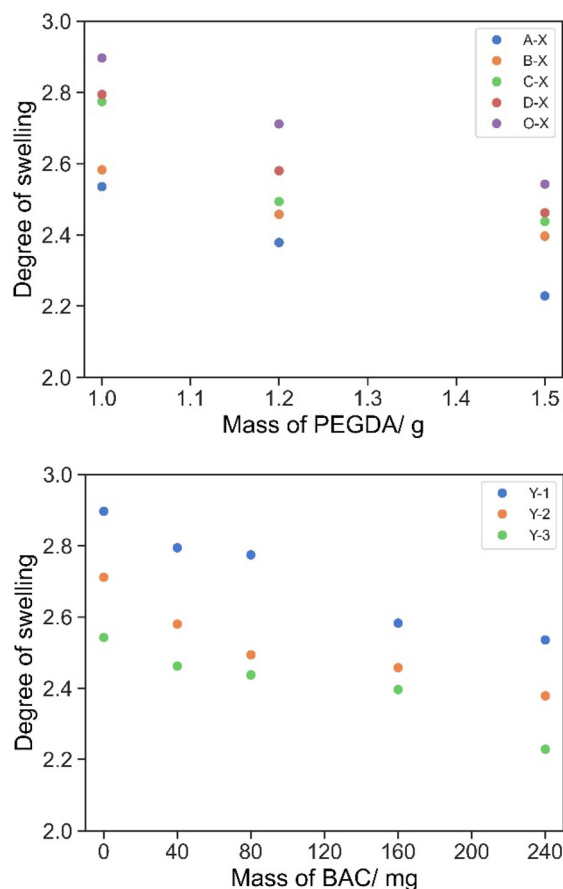
Fig. 3 The degree of swelling of cylinders A/B/C/D/O-1/2/3 compared with full hydration for 24 hours following drying at 30 °C for 48 hours. Top: grouped by the same BAC content and varying PEGDA contents in the *x*-axis; bottom: grouped by the same PEGDA content and varying BAC contents in the *x*-axis.

the higher the content of PEGDA or BAC, with the counterpart remaining at the same concentration, the lower the degree of swelling was observed, Fig. 3.

The hydrogel became softer after full hydration, the degree of swelling is the mass ratio of the completely swollen hydrogel to the sample mass and the change in the dimension of the hydrogel cylinder was calculated.

The degree of swelling of all formulations (Table 3) was important in the formulation to ensure that the printed cylinders fit in a plate reader for the designed experiment. The degree of swelling increased with a decrease in the concentration of PEGDA. At this level of swelling/hydration the swollen cylinders were suitable for use in the experiments. As the molar concentration of the disulphide crosslinker BAC is lower than that of PEGDA, the degree of swelling has no real significant change until it is >1 w/w%.

Release of tartrazine from the printed cylinders

Tartrazine is used to improve the print resolution by suppressing the spread of the irradiation during printing *via* reducing scattering and increasing localised absorption. The UV spec-

trum of tartrazine shows λ_{max} = 257 nm and 426 nm. The λ_{max} value of lanreotide = 277 nm of the residual tartrazine would interfere with the analysis and thus it was essential to remove the tartrazine prior to the measurement of reversible peptide conjugation. The UV-vis absorption of tartrazine in DI water is stable over 5 hours (ESI 3†) and the hydrogel was first incubated in a large excess of DI water for 5 h followed by changing the water and further incubation overnight. The amount of tartrazine released (Fig. 4) over 5 hours is calculated in Table 4. Following this the sample was washed to remove any residual material from the surface.

Glass transition temperature measurement

An increase in the amount of BAC or PEGDA in the formulated hydrogel resulted in a decrease in the glass transition temperature (T_g) (Fig. 5). Using PEGDA with M_{wt} = 700 and $T_g \approx -24$ °C and PHEA with $T_g \approx -10$ °C from the literature,[41,42] the T_g value of the blank sample (O-1/2/3) was found to be between the PEGDA and HEA homopolymer values, which decreases with an increase in the PEGDA content.

Table 3 Degree of swelling of all hydrogel formulations

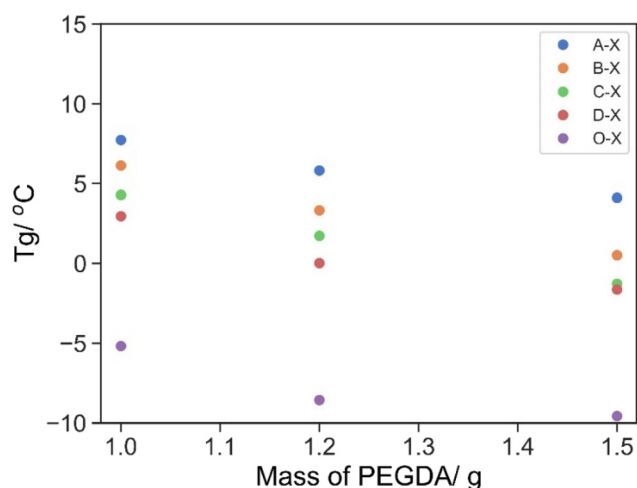|		Decreasing BAC content						
		A–X	B–X	C–X	D–X	F–X	H–X	O–X
Decreasing PEGDA content	Y-1	2.54	2.58	2.77	2.79	2.90	2.89	2.90
	Y-2	2.77	2.46	2.49	2.58	—		2.71
	Y-3	2.23	2.40	2.44	2.46	2.47		2.54
	Y-4	—	—	2.23	—	2.28	2.30	—
	Y-5	—	—	2.06	—	—		—
	Y-6	—	—	1.83	—	1.84	1.88	—
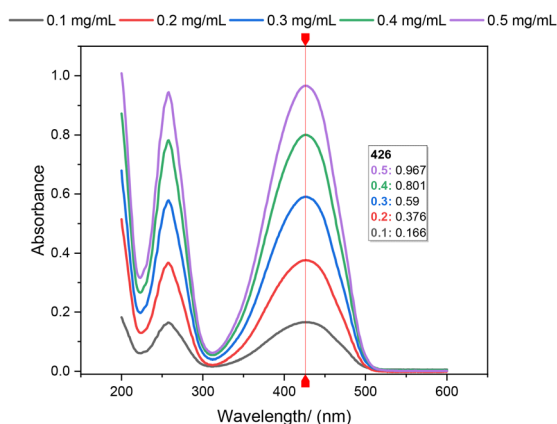
Fig. 4 Absorption of 160 μL tartrazine solution from 200 nm to 600 nm with concentration gradients of 0.1, 0.2, 0.3, 0.4, and 0.5 mg ml^{-1}.

Fig. 5 T_g (DSC) of series A/B/C/D/O-1/2/3. Grouped by the same BAC content and varying PEGDA contents in the x-axis (A: 240 mg, B: 160 mg, C: 80 mg, D: 40 mg and O: 0 mg BAC).

Table 4 Total amount of tartrazine released in 5 hours from printed cylinders of formulation (A/B/C/D-1/2/3)

Series				
PEGDA	A–X	B–X	C–X	D–X
Y-1	0.072 mg	0.031 mg	0.036 mg	0.033 mg
Y-2	0.059 mg	0.032 mg	0.034 mg	0.042 mg
Y-3	0.061 mg	0.029 mg	0.030 mg	0.037 mg

In comparison with the other series with BAC as the cross-linking agent (A/B/C/D), wherein the direct measurement of T_g of the BAC homopolymer is difficult due to the reversible di-sulfide exchange at elevated temperature, it was expected that the hydrogen bonding introduced by polyacrylamide along with the rigid crosslinking should increase T_g. Indeed, a higher T_g value was observed as the BAC content increased with the same PEGDA content, ESI Table 2.†

Evaluation of the thiol exchange kinetics

The printed parts were incubated with a TCEP solution for 24 h and the residual TCEP solution was removed by washing with DI water for a further 24 h. The parts were then trans-ferred to a 96 well plate for UV monitoring and 160 mL of 0.5 mM lanreotide solution was added to the hole within the cylinders, allowing for monitoring of the UV spectrum through the hole in the plate reader. The absorbance at λ = 277 nm was

monitored over 2.5 h. Subsequently, a portion of the solution was removed and replaced with 160 mL of 10 mM TCEP solu-tion. This leads to the release of lanreotide *via* disulphide reduction as monitored by the change in absorbance at 277 nm. The coupling and release studies were first validated by three repetitions using F-5 as an example, and it demon-strated good repeatability in both processes (Fig. 6).

Then, the effect of BAC in this process was evaluated by comparing the controls with the resin without BAC (O-1/2/3) and with BAC (D-1/2/3). In the absence of BAC, the uptake of lanreotide was incomplete over the 180 min monitoring period, with a maximum of 74% uptake in the least cross-linked material (O-1). This process exhibited 2 stages with a rapid decline in the absorbance observed over the first 60 min followed by a more gradual reduction in the second stage. A total of 90% lanreotide uptake was observed within 60 min regardless of the crosslink density (Fig. 7).

Thus, the release profiles with a concentration of <0.1 mM in all cases showed no significant differences with changes in the crosslink density without BAC. In the presence of BAC, the released lanreotide remained >0.5 mM and approximately twice as much as in the control at all crosslink densities studied. Thus, BAC allows for the conjugation of lanreotide *via*
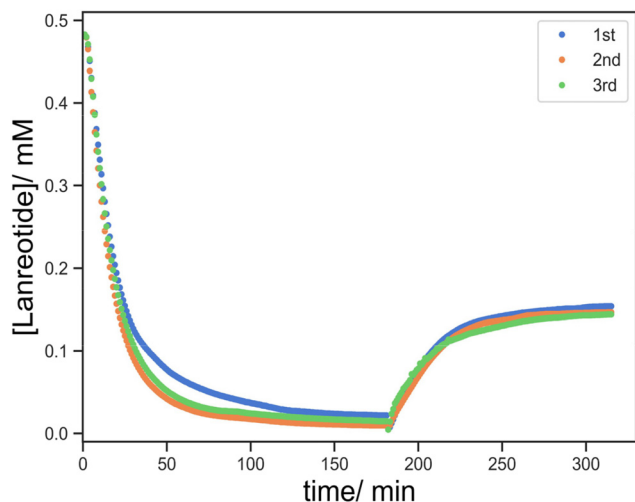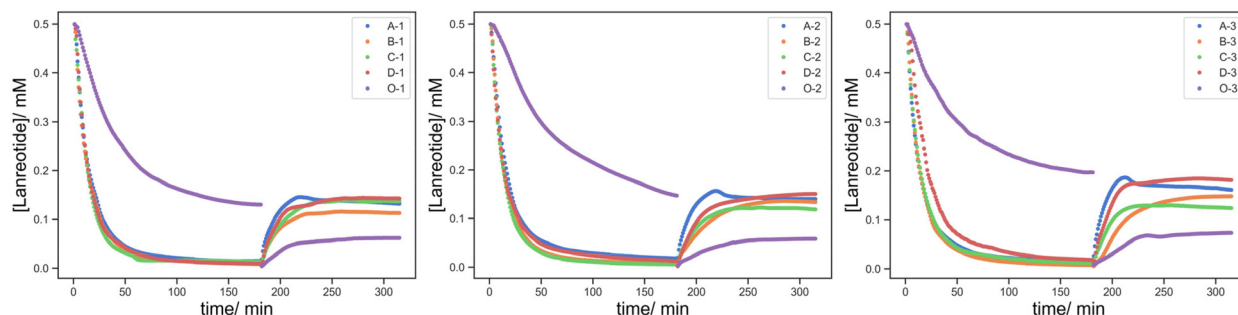
Fig. 6 Three repetitions of lanreotide uptake and release profiles for the repeatability test using F-3 as an example.
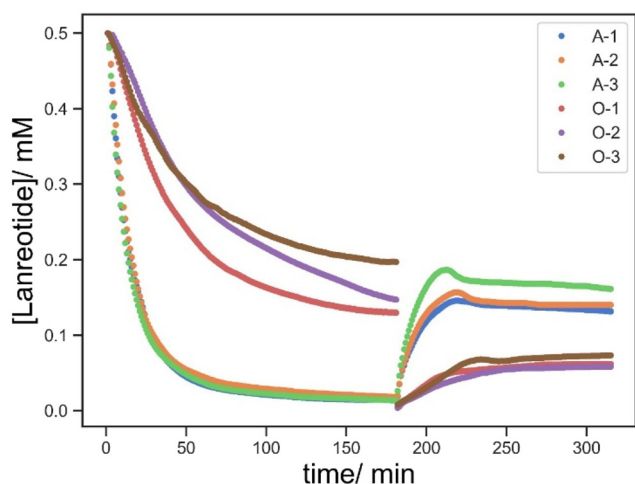
Fig. 7 [Lanreotide] *vs.* time of A-1 (blue), A-2 (orange), A-3 (green) and the control without BAC O-1 (red), O-2 (purple) and O-3 (brown). The first 180 min shows the uptake process followed by the addition of 0.5 mM lanreotide solution to the well and the latter 180 min shows the release process followed by the addition of 10 mM TCEP solution.

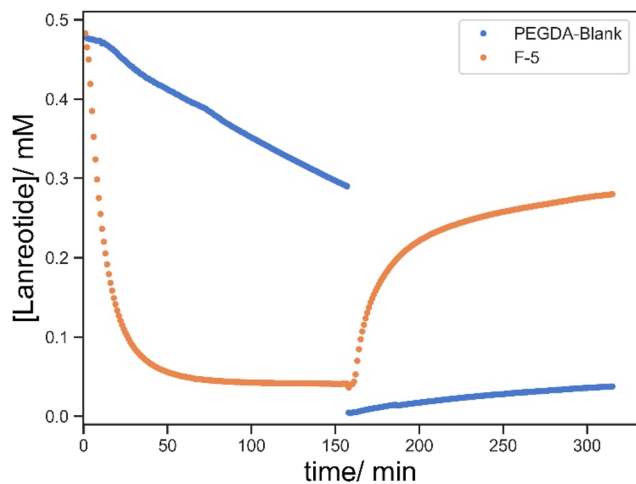covalent bond formation and uptake is not only by physical absorption.

The effect of the BAC content on the materials properties is relatively complicated due to the considerations of the cross-link density and re-conjugation *via* dynamic thiol disulfide exchange, especially the decrease in the [lanreotide] in the second stage (Fig. 8). Whilst the effect of BAC on this process of the release cannot be explained by simple diffusion theory, it is clear that both the quantity of uptake and release of lanreotide is significantly enhanced by the incorporation of a disulphide containing BAC crosslinking agent.

Thus, no significant change in the uptake and release profiles was due to the high [BAC] : [Lanreotide] and low crosslink density with the effect of the hydrogel pore size being minimal. To understand the peptide uptake and release processes in terms of both the crosslinking density and BAC content similar parts were printed in the absence of HEA as the diluent monomer (*PEGDA-blank* and *E-1*).

The uptake and release profiles of PEGDA-blank (no BAC) and E-1 (2 mg BAC) are shown in Fig. 9. Firstly, the lanreotide concentration reduces rapidly in the presence of BAC due to covalent incorporation *via* disulfide bonds (*E-1*) whilst decreasing at a slower and more linear way in the absence of BAC (PEGDA-blank) over the first 15 min due to non-covalent interactions. This suggests that lanreotide predominantly conjugates *via* covalent bond formation at the $-SH$ groups. Following this 15 min induction period, the lanreotide concentration gradually declined in the absence of BAC (*PEGDA-blank*) suggesting that lanreotide was still able to diffuse into the printed object even with a higher crosslink density.

Compared to the low-crosslinked materials in the absence of BAC (O-1/2/3; 5 : 1.0/1.2/1.5 w/w of HEA : PEGDA700), the rate of lanreotide uptake increases with a corresponding decrease in the crosslink density (PEGDA : HEA) (Fig. 10), ascribed to easier diffusion through the looser network and smaller pore size. The release from all non-BAC containing samples is much more modest due to the lack of disulphide conjugation of lanreotide thus not susceptible to cleavage *via* TCEP reduction.

Fig. 8 [Lanreotide] *vs.* time of (*Series*-1 (left)/2 (middle)/3 (right)–A (blue)/B (orange)/C (green)/D (brown)/O (purple)). The first 180 min shows the uptake process followed by the addition of 0.5 mM lanreotide solution to the well and the latter 180 min shows the release process followed by the addition of 10 mM TCEP solution.

© 2024 The Author(s). Published by the Royal Society of Chemistry

*RSC Appl. Polym.*, 2024, **2**, 415–425 | **421**

Fig. 9 [Lanreotide] *vs.* time of crosslinked PEGDA only F-5 (blue) with BAC and PEGDA-blank (orange) without BAC. The first 150 min refers to the uptake process followed by the addition of 0.5 mM lanreotide solution and the subsequent 180 min shows the lanreotide release followed by the replacement of the solution with 10 mM TCEP solution.
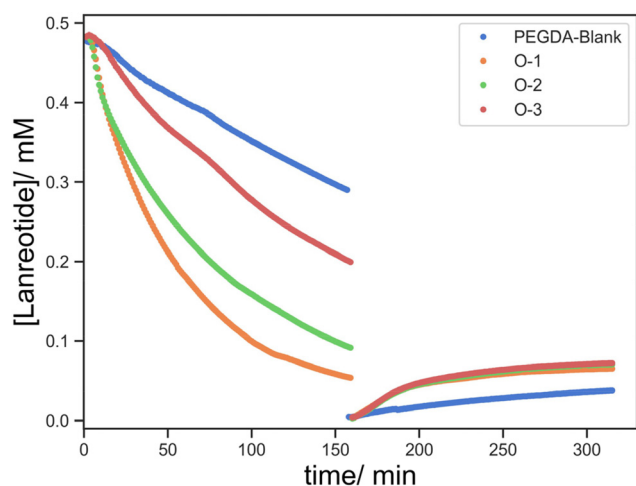
Fig. 10 [Lanreotide] *vs.* time of samples without BAC at different crosslink densities: PEGDA-blank (blue), O-1 (orange), O-2 (green) and O-3 (brown). The first 150 min refers to the uptake process followed by the addition of 0.5 mM lanreotide solution and the subsequent 180 min shows the lanreotide release followed by replacing the solution with 10 mM TCEP solution.

It seems that the uptake of lanreotide into the printed object can occur *via* at least two pathways. Initially, lanreotide reacts with the free thiols from the reduced BAC on the surface of the printed object in a rapid process that is governed by the BAC concentration in the formulation and is largely independent of the crosslink density. The series with a lower content of BAC, F-1/2/3/4 (5 : 1/1.5/2/5 HEA : PEGDA), shows two different release steps (Fig. 11 top). In the first 30 min, the rate of lanreotide release is independent of the crosslinker concentration, attributed to the rapid release from the surface and the crosslink density is negligible for this process.
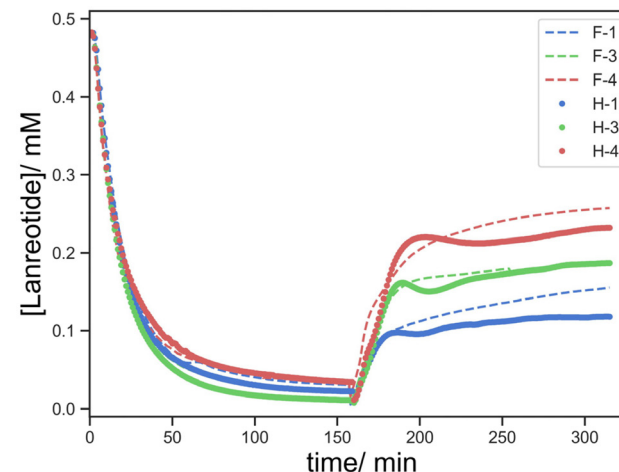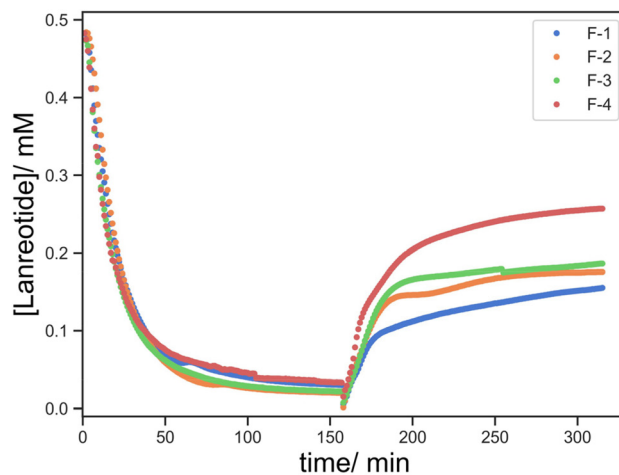
Fig. 11 [Lanreotide] *vs.* time of F-1/2/3/4 (top) and F (solid line)/H (dotted line)-1/3/4 (bottom) to compare the effect of the BAC content on the uptake process (F: 2 mg BAC, H: 0.2 mg BAC). The first 150 min refers to the uptake process followed by the addition of 0.5 mM lanreotide solution and the subsequent 180 min shows the lanreotide release followed by replacing the solution with 10 mM TCEP solution.

Subsequently, diffusion-controlled release within the printed object predominates, and the crosslink density affects this process. The rate of release of lanreotide surprisingly increases at a higher crosslink density. We offer the explanation that despite similar uptake profiles, the diffusion of lanreotide inside the hydrogel/printed object is different with a different crosslink density. As the crosslink density is reduced lanreotide migrates faster into the core of the part *via* both diffusion and thiol–disulfide exchange, and the lanreotide accumulated at the surface is reduced. As a result, in the release process the initial rapid release from the surface is more significant and the total released lanreotide is the maximum at the highest crosslink density studied.

When compared to the effect of the BAC content (Fig. 11 bottom), F-1/2/3 (0.2 mg BAC) *vs.* H-1/2/3 (0.2 mg BAC), while the uptake process occurs at a very similar rate, the amount of lanreotide released was higher at a higher BAC content. It seems that the higher the BAC content more lanreotide conju-

422 | *RSC Appl. Polym.*, 2024, **2**, 415–425

© 2024 The Author(s). Published by the Royal Society of Chemistry

gates to the hydrogel printed part and is subsequently released upon reduction with TCEP. Moreover, the release profile at a lower BAC content shows a more complex "*wave*" feature which seems to somewhat self-correct. This is ascribed to a time lag between the surface and bulk release becoming larger at lower [BAC]. Initially, the release from the surface predominates over from the bulk material, and this was more pronounced at low [BAC]. The wave-like feature diminishes as the time lag by the diffusion from the core to the surface is overcome.

To decouple the absorption by physical diffusion and actual chemical conjugation, the highest crosslink density material (E-1) was chosen (Fig. 12). It was expected that in the non-treated printed part the absorption and release of lanreotide were both predominant *via* diffusion, whereas the TCEP-treated sample absorbed lanreotide *via* both chemical conjugation and diffusion. To validate this, the hydrogel treated with TCEP showed complete absorption of lanreotide and then water and TCEP solution were added to two identical TCEP-treated hydrogels to determine whether the lanreotide was chemically conjugated.

No lanreotide was released by the addition of water, as contrasted to the blank where free lanreotide in solution by diffusion was detected, suggesting that the lanreotide was chemically conjugated to the printed part. Only when TCEP solution was added, the release of lanreotide was significantly increased relative to the non-treated sample, again suggesting that the lanreotide was predominantly absorbed by the hydrogel *via* chemical bonding instead of physical swelling. This also gives insight into the uptake mechanism that while the diffusion of lanreotide into the hydrogel assisted its uptake significantly, the lanreotide was eventually conjugated to the printed part *via* thiol–disulfide exchange once it reached inside the hydrogel.
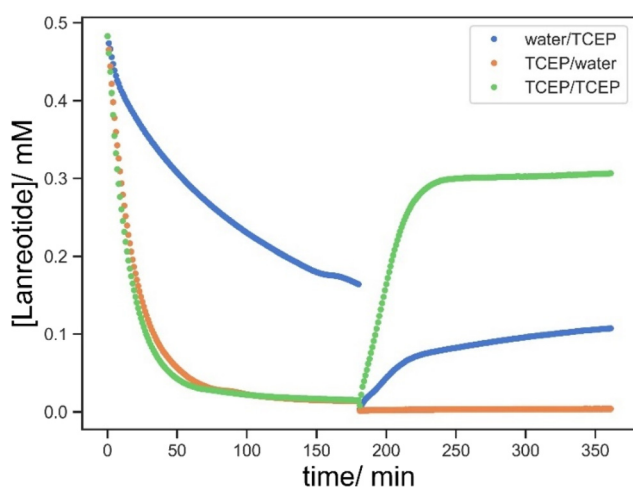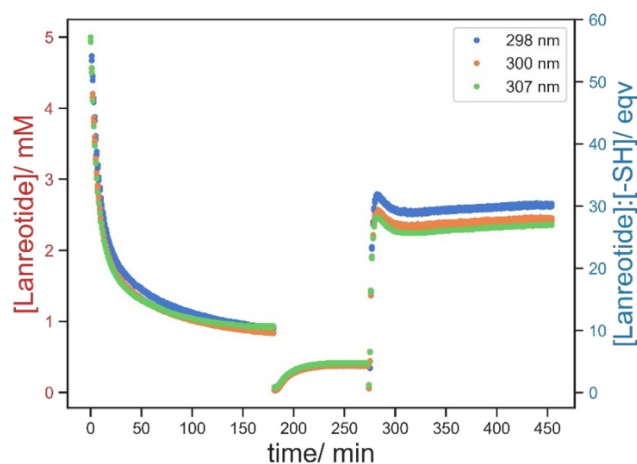
Then water was added to evaluate the release of free lanreotide. Although unbound lanreotide was now detectable at this low BAC content in printed parts and high lanreotide concentration, it only contributed to 10% of the total absorbed lanreotide and the rest was released only by the subsequent addition of TCEP solution. This demonstrated an unexpected phenomenon that the conjugation of lanreotide surpassed the theoretical BAC content in the printed parts (Fig. 13). One of the plausible explanations was the ring opening polymerization of lanreotide *via* a disulfide linkage. This was favoured in the hydrogel but not in solution owing to the conformational confinement minimizing the depolymerization by another free ring-opened lanreotide. However, the mechanism requires further investigation.

The quantification of thiol groups in the hydrogel was attempted by the use of Ellman's reagent. However, this method involves the reversible thiol–disulfide exchange, and the reaction kinetics and the equilibrium of the reaction depend on the thiol type, local concentration, and other environmental factors, which normally will be corrected by calibration. For solid samples, it is difficult to prepare a valid calibration to correct these factors using current well-plate UV absorption measurement, and this eventually led to inaccurate quantification from the measured values.
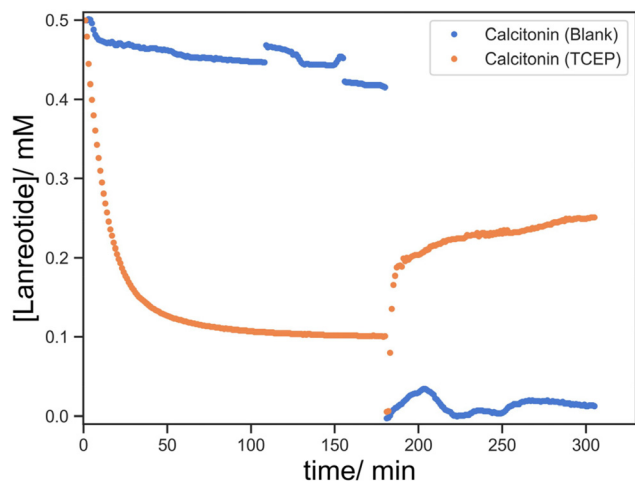
Universality of DLP-printed loading parts

Lastly, the versatility of the thiol–disulfide functionalized objects *via* DLP printing was demonstrated. For the chemical functionality, a preliminary demonstration of the absorption and release of calcitonin, another cyclic disulfide containing peptide, was performed using F-3. We successfully demonstrated the conjugation and redox-triggered release of calcitonin enabled by thiol–disulfide exchange, whereas the blank

Fig. 12 [Lanreotide] *vs.* time of E-1 pretreated with water (blue); E-1 pretreated with TCEP solution (orange and green). The first 180 min show the uptake process by adding 0.5 mM lanreotide solution to the well and the latter 180 min show the release process followed by the addition of 10 mM TCEP solution (blue and green) or water (orange).

Fig. 13 [Lanreotide] and its equivalence to theoretical thiol groups on H-3 *vs.* time monitored by the absorbance at 298 nm (blue), 300 nm (orange) and 307 nm (green). The first 180 min show the uptake process followed by adding 5 mM lanreotide solution to the well, the next 90 min show the leaching process of free lanreotide followed by the addition of water, and then the last 180 minutes show the release process by the addition of 10 mM TCEP solution.

© 2024 The Author(s). Published by the Royal Society of Chemistry

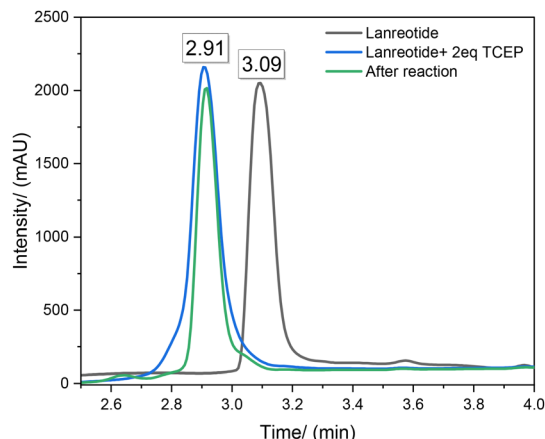*RSC Appl. Polym.*, 2024, **2**, 415–425 | **423**

Fig. 14 Combination and release profiles of calcitonin using blank (blue) and TCEP-treated (orange) F-3. Fluctuations in the blank were attributed to the inclusion of gas bubbles during the measurements.

Fig. 16 RP-HPLC chromatograms of sample: 0.5 mM Lanreotide (black) and 0.5 mM Lanreotide with 2equiv. of 0.5 mM TCEP-HCl (blue) and lanreotide released following the reaction (green).

showed insignificant absorption and thus release (Fig. 14). While similar profiles were observed in calcitonin, there were certain disparities between calcitonin and lanreotide in the absolute quantities of the absorbed and released peptides, which were possibly attributed to the difference in the peptide structures and the reactivity of the disulfide in the individual peptide. Overall, it highlighted the adaptability of thiol-functionalized printing for the loading and delivery of various disulfide-containing molecules.

Considering DLP as a processing method, different complex structures, with internal channels (filled with cochineal solution for clarity), have been printed (Fig. 15). This demonstrated the capability for DLP printing to manufacture objects with a tortuous geometry. This signified its potential applications in scaffolding or implanting where refined architecture is required.

Determination of lanreotide release using RP-HPLC

In addition to monitoring the UV-absorption, reverse phase-high performance liquid chromatography (RP-HPLC) was used to determine the efficiency of TCEP as a cleaving agent in the hydrogel system. Fig. 16 shows the chromatograms of lanreotide before (black) and after (blue) treatment with TCEP. After the cleavage of disulfide by TCEP, the retention time of lanreotide shifts from 3.09 min to 2.91 min with the ring opened form. Then, the residual solution of A-3 was taken, as an example, characterized by RP-HPLC (green) and eluted at 2.91 min without traces at 3.09 min, suggesting that the release of lanreotide was in this ring opened form. Complementary to the UV data, this further supported the fact that lanreotide was released by cleavage of THE disulfide linkage with the printed parts instead of physical leaching.

Conclusion

We demonstrate the successful manufacture of hydrogel objects with significant quantities of water with good resolution crosslinked with a disulfide containing crosslinker using DLP 3D printing. Reduction of the disulfides to thiols followed by subsequent thiol–disulfide peptide exchange allowed for successful covalent incorporation of lanreotide (as an exemplar for a peptide containing a disulphide or free thiol) into these objects. This covalent binding has been shown to be reversible, and the peptide is released by a second reduction of the disulfide. The rate of release can be somewhat controlled by the amount of disulphide groups incorporated and the total crosslink density. Thus, we believe that the crosslink density and BAC content can be used to control the extent of swelling of the hydrogel leading to the control of hardness/softness uptake and release of peptides containing disulfides. These materials show potential for the fabrication of devices and/or implants which are capable of reversible covalent attachment of peptides with different loading and controlled release properties with prescribed and diverse biological activities.

Fig. 15 Examples of DLP-printed objects with internal channels or a refined geometry demonstrating their capability for fabricating high resolution objects.

424 | *RSC Appl. Polym.*, 2024, **2**, 415–425

© 2024 The Author(s). Published by the Royal Society of Chemistry

Conflicts of interest

Ataulla Shegiwal and David Haddleton are shareholders and Directors of Halcyon 3D Ltd.

References

1 E. A. Guzzi and M. W. Tibbitt, *Adv. Mater.*, 2020, **32**, 1901994.

2 B. Grigoryan, S. J. Paulsen, D. C. Corbett, D. W. Sazer, C. L. Fortin, A. J. Zaita, P. T. Greenfield, N. J. Calafat, J. P. Gounley, A. H. Ta, F. Johansson, A. Randles, J. E. Rosenkrantz, J. D. Louis-Rosenberg, P. A. Galie, K. R. Stevens and J. S. Miller, *Science*, 2019, **364**, 458–464.

3 H.-W. Kang, S. J. Lee, I. K. Ko, C. Kengla, J. J. Yoo and A. Atala, *Nat. Biotechnol.*, 2016, **34**, 312–319.

4 R. L. Truby and J. A. Lewis, *Nature*, 2016, **540**, 371–378.

5 J. Li, C. Wu, P. K. Chu and M. Gelinsky, *Mater. Sci. Eng., R*, 2020, **140**, 100543.

6 T. D. Ngo, A. Kashani, G. Imbalzano, K. T. Q. Nguyen and D. Hui, *Composites, Part B*, 2018, **143**, 172–196.

7 W. Zhu, X. Ma, M. Gou, D. Mei, K. Zhang and S. Chen, *Curr. Opin. Biotechnol.*, 2016, **40**, 103–112.

8 X. Peng, X. Kuang, D. J. Roach, Y. Wang, C. M. Hamel, C. Lu and H. J. Qi, *Addit. Manuf.*, 2021, **40**, 101911.

9 J. Huh, Y.-W. Moon, J. Park, A. Atala, J. J. Yoo and S. J. Lee, *Biofabrication*, 2021, **13**, 034103.

10 S. C. Ligon, R. Liska, J. Stampfl, M. Gurr and R. Mülhaupt, *Chem. Rev.*, 2017, **117**, 10212–10290.

11 H. Hong, Y. B. Seo, D. Y. Kim, J. S. Lee, Y. J. Lee, H. Lee, O. Ajiteru, M. T. Sultan, O. J. Lee, S. H. Kim and C. H. Park, *Biomaterials*, 2020, **232**, 119679.

12 M. Caprioli, I. Roppolo, A. Chiappone, L. Larush, C. F. Pirri and S. Magdassi, *Nat. Commun.*, 2021, **12**, 2462.

13 Y. Lu, G. Mapili, G. Suhali, S. Chen and K. Roy, *J. Biomed. Mater. Res., Part A*, 2006, **77A**, 396–405.

14 F. P. W. Melchels, M. A. N. Domingos, T. J. Klein, J. Malda, P. J. Bartolo and D. W. Hutmacher, *Prog. Polym. Sci.*, 2012, **37**, 1079–1104.

15 C. J. Ferris, K. G. Gilmore, G. G. Wallace and M. In het Panhuis, *Appl. Microbiol. Biotechnol.*, 2013, **97**, 4243–4258.

16 S. V. Murphy and A. Atala, *Nat. Biotechnol.*, 2014, **32**, 773–785.

17 M. Zhang, R. Lin, X. Wang, J. Xue, C. Deng, C. Feng, H. Zhuang, J. Ma, C. Qin, L. Wan, J. Chang and C. Wu, *Sci. Adv.*, 2020, **6**, eaaz6725.

18 B. Derby, *Science*, 2012, **338**, 921–926.

19 J. Zhang, Q. Hu, S. Wang, J. Tao and M. Gou, *Int. J. Bioprint.*, 2019, **6**, 242.

20 S. N. Economidou, D. A. Lamprou and D. Douroumis, *Int. J. Pharm.*, 2018, **544**, 415–424.

21 S. Beg, W. H. Almalki, A. Malik, M. Farhan, M. Aatif, Z. Rahman, N. K. Alruwaili, M. Alrobaian, M. Tarique and M. Rahman, *Drug Discovery Today*, 2020, **25**, 1668–1681.

22 J. Zhang, A. Q. Vo, X. Feng, S. Bandari and M. A. Repka, *AAPS PharmSciTech*, 2018, **19**, 3388–3402.

23 *Strategies to Modify the Drug Release from Pharmaceutical Systems*, ed. M. L. Bruschi, Woodhead Publishing, 2015, pp. 87–194.

24 N. A. Elkasabgy, A. A. Mahmoud and A. Maged, *Int. J. Pharm.*, 2020, **588**, 119732.

25 D. Yang, W. Chen and J. Hu, *J. Phys. Chem. B*, 2014, **118**, 12311–12317.

26 A. Shastri, L. M. McGregor, Y. Liu, V. Harris, H. Nan, M. Mujica, Y. Vasquez, A. Bhattacharya, Y. Ma, M. Aizenberg, O. Kuksenok, A. C. Balazs, J. Aizenberg and X. He, *Nat. Chem.*, 2015, **7**, 447–454.

27 T. N. Gevrek, M. Cosar, D. Aydin, E. Kaga, M. Arslan, R. Sanyal and A. Sanyal, *ACS Appl. Mater. Interfaces*, 2018, **10**, 14399–14409.

28 W. Sheng, T. Chen, R. Kamath, X. Xiong, W. Tan and Z. H. Fan, *Anal. Chem.*, 2012, **84**, 4199–4206.

29 A. A. Adams, P. I. Okagbare, J. Feng, M. L. Hupert, D. Patterson, J. Göttert, R. L. McCarley, D. Nikitopoulos, M. C. Murphy and S. A. Soper, *J. Am. Chem. Soc.*, 2008, **130**, 8633–8641.

30 A. Hatch, G. Hansmann and S. K. Murthy, *Langmuir*, 2011, **27**, 4257–4264.

31 C. R. Fellin and A. Nelson, *ACS Appl. Polym. Mater.*, 2022, **4**, 3054–3061.

32 H. A. Aliyar, P. D. Hamilton and N. Ravi, *Biomacromolecules*, 2005, **6**, 204–211.

33 R. Zhang, T. Nie, Y. Fang, H. Huang and J. Wu, *Biomacromolecules*, 2022, **23**, 1–19.

34 I. Altinbasak, M. Arslan, R. Sanyal and A. Sanyal, *Polym. Chem.*, 2020, **11**, 7603–7624.

35 R. Bej, P. Dey and S. Ghosh, *Soft Matter*, 2019, **16**, 11–26.

36 R. Kilic Boz, D. Aydin, S. Kocak, B. Golba, R. Sanyal and A. Sanyal, *Bioconjugate Chem.*, 2022, **33**, 839–847.

37 A. M. Klein, L. Mazutis, I. Akartuna, N. Tallapragada, A. Veres, V. Li, L. Peshkin, D. A. Weitz and M. W. Kirschner, *Cell*, 2015, **161**, 1187–1201.

38 B. Zachary, M. Elliott, R. Daniel, R. Paul and S. Niranjan, US10745742, 2020.

39 O. Muratoglu, S. Spiegelberg, J. Ruberti and N. Abt, US7985781, 2011.

40 A. Charlet, M. Hirsch, S. Schreiber and E. Amstad, *Small*, 2022, **18**, 2107128.

41 J. Zhang, F. She, W. Gao and L. Kong, in *5th IWA Specialised Membrane Technology Conferences for Water and Wastewater Treatment*, Tsinghua University, Beijing, China, 2009, pp. ID233–ID233.

42 J. Rault, A. Lucas, R. Neffati and M. Monleón Pradas, *Macromolecules*, 1997, **30**(25), 7866–7873.

© 2024 The Author(s). Published by the Royal Society of Chemistry

RSC Appl. Polym., 2024, **2**, 415–425 | **425**